Bioorganic Chemistry 153 (2024) 107836

Contents lists available at ScienceDirect

Bioorganic Chemistry

journal homepage: www.elsevier.com/locate/bioorg

Glycoconjugate coumarins exploiting metabolism-enhanced fluorescence and preferential uptake: New optical tools for tumor cell staining

Dalila Iacopini [a,1], Melissa Santi [b,1], Maria Chiara Santangelo [a], Gemma Sardelli [c], Lucia Piazza [c,d], Rossella Mosca [c], Lucrezia Margherita Comparini [a], Carlotta Granchi [a], Mauro Pineschi [a], Sebastiano Di Pietro [a,*], Giovanni Signore [c,d,e,*], Valeria Di Bussolo [a]

[a] *Department of Pharmacy, University of Pisa, Via Bonanno Pisano 33, 56126 Pisa, Italy*
[b] *Istituto Nanoscienze-CNR, NEST Laboratory, Piazza San Silvestro 12, 56127 Pisa, Italy*
[c] *Biochemistry Unit, Department of Biology, University of Pisa, 56123 Pisa, Italy*
[d] *Institute of Clinical Physiology, National Research Council, 56124 Pisa, Italy*
[e] *Interdepartmental Research Center Nutrafood "Nutraceuticals and Food for Health", University of Pisa, 56123 Pisa, Italy*

ABSTRACT

The possibility to visually discriminate cells based on their metabolism and capability to uptake exogenous molecules is an important topic with exciting fallback on translational and precision medicine. To this end, probes that combine several complementary features are necessary. The ideal probe is selectively uptaken and activated in tumor cells compared with control ones and is not fluorescent in the extracellular medium. Fluorogenic compounds that combine enzyme-activated pH sensitivity and good cell uptake can be an ideal solution, provided that the sensed enzymes are dysregulated in tumor cells. Here, we present synthesis and *in vitro* evaluation of a new class of glyco-coumarin based probes that merge all these features. These probes show uptake ratio in tumor vs. control cells up to 3:1, with a cell to background ratio upon administration of the probe up to 5:1. These features make this new family of fluorogenic targeted probes a promising tool in life science.

1. Introduction

Tumor cells are characterized by aberrant metabolic state due to the need to comply with their replicative status.[1] In keeping with the high proliferative activity of tumor cells, metabolism is redirected towards a glycolytic mechanism that improves cell resistance to increased ROS production and provides a better metabolic balance for the synthesis of biomolecule building blocks. This phenomenon, referred to as "Warburg effect", [2,3] is one of the bases for the increased glucose uptake in tumor sites (the other being the common, albeit not universal, hypoxic state of tumor microdomains). Regardless of the cause, switch to a glycolytic mechanism [4] and high proliferation rate cause significant increase in glucose uptake that is reflected in the common overexpression of glucose transporters in tumor cells compared with physiologic conditions.[5] This effect has been widely exploited in diagnostic medicine to evaluate the presence of tumors by PET scan with 18F-deoxyglucose, whose accumulation provides a clear clinical indication of tumor site and dimensions.[6–8] Another immediate consequence of switch to a glycolytic metabolism is represented by the altered pH in tumor cells [9] and microenvironment,[10] due to altered metabolism excess production and excretion of lactic acid,[11,12] and functional alteration of key enzymes such as pyruvate kinase,[13,14] which further promotes metabolism shift towards glycolysis. Notably, most of these aspects are actually intertwined, with a major role played by altered redox level in cells,[15] giving rise to synergistic activity between different cell components. This feature led to the identification of intracellular and extracellular pH as a key parameter in the identification of tumor cells,[16,17] and provided interesting hints for selective, or at least preferential, tumor treatment.[18]

Despite its exquisite sensitivity and widespread use in diagnostic medicine, glucose uptake imaging finds a bottleneck in the applicability to emerging techniques such as intra-operative monitoring of tumor cells and enhanced vision surgery.[19] Fluorescence-guided approaches are, in this context, the most promising ones due to the unique combination of sensitivity, spatial resolution, and low risks for surgical staff, with several examples emerging from base science [20,21] and clinical literature.[21–24] The high sensitivity of fluorescence-based techniques, and the possibility to assemble probes which are sensitive to the external environment, make fluorescent solvatochromic dyes an excellent candidate to allow precise localization of malignant cells. Despite

* Corresponding authors.
E-mail addresses: sebastiano.dipietro@unipi.it (S. Di Pietro), giovanni.signore@unipi.it (G. Signore).

[1] Equal contribution

https://doi.org/10.1016/j.bioorg.2024.107836
Received 22 July 2024; Received in revised form 16 September 2024; Accepted 18 September 2024
Available online 19 September 2024

the availability of well suited fluorescent probes for image-guided surgery, there is an increasing need to gain access to specific, bright, and metabolically orthogonal probes able to improve signal to noise ratio and, ultimately, overall efficiency.[25] In this view, the already discussed presence of multiple altered features in tumor cells could be exploited in triggering a more pronounced effect. In this view, overexpression of glucose transporters,[5] altered extracellular and intracellular pH,[26] and altered glucosidase expression and activity [27] could be considered. Thus, it is not surprising that several activatable fluorescent probes have been developed and tested recently. Both pH sensitive probes [28] and glycoside-functionalized dyes have been exploited in current research. pH sensitive probes have been evaluated *in vitro* [29] and *in vivo*.[30] On the other end, glycosidase [31] and mannosidase [32] sensitive probes have recently described in the literature, in line with the more general strategy of using enzyme-activatable probes for tumor imaging.[33] This strategy is even more powerful when multiple orthogonal stimuli (photochromic activation) [34,35] are combined, as highlighted from recent literature reviews.[36] Obviously, the use of glucose-conjugated dyes would be a game-changer in such procedures, due to the possibility to match an optical readout with a metabolic fingerprint of tumor cells. Notably, the strategy of combining two stimuli (β-galactosidase sensitivity and pH-dependent fluorescence) was recently exploited in the development of a new activatable, tumor targeted probe,[37] and some exciting results have been obtained conjugating mannitol and fluorescent coumarins.[38] Conventional carbohydrate-dye conjugates are however poorly fit to address this issue, due to their constant fluorescence regardless of the environment, that would mask the contrast between cellular and extracellular environment. Solvatochromic, enzyme activated probes, on the other hand, would exploit a double leverage effect due to preferential uptake in tumor cells and increased fluorescence readout only after enzymatic cleavage in the intracellular environment. Activatable glycoconjugate probes have been recently described that exploits pH changes in cells compared with the external medium.[39] In this view, contrast between physiologic and pathologic tissue can be maintained, and even increased, due to a signalling cascade from the exterior and intracellular part of the cell. Based on our long history on environmentally sensitive coumarin derivatives,[40–42] synthesis of fluorescent bioprobes,[43] and on the *in vitro* evaluation of glycoconjugates,[44] we envisaged that a combination of these two components could provide exceptional sensitivity to distinguish between tumor and physiologic cells.

The experimental plan involved design and synthesis of three fluorogenic probes to evaluate their: i) sensitivity to enzymatic digestion; ii) subcellular localization, and iii) ability to distinguish between tumoral and control cells with a simple no-wash optical assay.

2. Materials and Methods

2.1. Materials and methods

All solvents and chemicals were purchased from Merck and used without further purification. All reactions were performed in a flame-dried modified Schlenk (Kjeldahl shape) flask fitted with a glass stopper or rubber septum under a positive pressure of argon. Purifications were performed on silica gel columns by flash chromatography (Kieselgel 40, 0.040–0.063 mm; Merck) or by LC chromatographic Biotage Isolera Four (Biotage, Uppsala, Sweden) preparative purification system. Reactions were followed by thin-layer chromatography (TLC) on Merck aluminum silica gel (60 F254) sheets that were visualized under a UV lamp. Evaporation was performed *in vacuo* (rotating evaporator). Sodium sulfate was used as drying agent. Yields refer to isolated and purified products. 1D and 2D-NMR were recorded with a Bruker Avance III 400 MHz spectrometer (Bruker, Billerica, MA, USA), using the indicated deuterated solvents. Chemical shifts are given in parts per million (ppm) (δ relative to residual solvent peak for ^{1}H and ^{13}C). HPLC purity of compounds were determined using a Waters Alliance 2695 equipped with a 2420 dual wavelength detector (Waters, Milford, MA, USA) using the following parameters: column Phenomenex Luna C8 150 mm × 3 mm × 5 μm (Phenomenex, Torrance, CA, USA), mobile phases water/TFA 100/0.01 v/v and Acetonitrile 100 v/v. Retention times (HPLC, t_R) are given in minutes. Compound HPLC purity was evaluated at 254 nm. The ESI-MS spectrum was recorded by direct injection at 7 μL min/1 flow rate in an Orbitrap high-resolution mass spectrometer (Thermo, San Jose, CA, USA), equipped with H-ESI source. The working conditions were as follows: negative polarity, spray voltage − 3.2 kV, capillary temperature 290 °C, S-lens RF level 50. The sheath and the auxiliary gases were set at 28 and 4 (arbitrary units), respectively. For acquisition and analysis, Xcalibur 4.2 software (Thermo) was used. For spectra acquisition a nominal resolution (at *m/z* 200) of 140 000 was used.

Detailed description of synthetic procedures is provided in supporting information

2.2. Fluorescence measurements

Emission spectra were recorded by means of a Cary Eclipse fluorometer (Varian, Palo Alto, CA). The temperature of the cell compartment was controlled by a built-in Peltier cooler (Varian) and maintained at 37 °C. Excitation and emission band-pass of 10 nm was employed. All the compounds were excited at 405 nm and the fluorescence emission was recorded from 410 nm to 600 nm. A stock solution of each compound (1 mM in DMSO) was diluted in the appropriate buffer solution for enzyme activity measurements to the final concentration of 10 μM. Buffer solution was made of 0.4 M disodium hydrogen phosphate and 0.2 M citric acid (pH 6.5). The right amount of enzyme (α-glucosidase, β-glucosidase or α- mannosidase, all from Sigma-Merk) was added to the solution and the fluorescence signal was measured every 5 min.

2.3. Cell cultures and in vitro experiments

GL261 and MEF cell lines were cultured in Dulbecco's modified Eagle medium (DMEM) high glucose (Gibco) with 10 % fetal bovine serum, 4 mM l-glutamine, 1 mM sodium pyruvate, 100 U/ml penicillin, and 100 mg/mL streptomycin (Invitrogen). Cells were maintained at 37 °C with 5 % of CO_2 until their use. Cells were trypsinized and then seeded in the appropriate plate according to the type of experiment. For confocal microscopy 2×10^5 cells were seeded in Willco dishes (35-mm diameter) for 24 h and then treated with 10 or 100 μM of compound (stock solution was properly diluted to obtain a maximum DMSO percentage of 1 %) and 100 nM of Lysotracker Deep-Red (LifeTechnologies) for 1 h. Then cells were washed twice with PBS and fresh medium was added before imaging. For quantitative uptake measurements, 1×10^4 cells were seeded in a black 96-wells plate with a glass bottom for fluorescent measures (Thermo Fisher Scientific); after 24 h cells were treated with 10 or 100 μM of compounds. To better understand the rate of internalization of the compounds we treated both cell lines with DMEM with low or high glucose content. Internalization rate was measured with a microplate reader (Promega, GloMax discover Multimode microplate reader) with excitation filter 405 nm and emission filter 415–445 nm, 415–485 nm and 500–550 nm.

2.4. Confocal microscopy

After incubation with each compound, cells were washed twice with PBS and imaged with a Zeiss LSM 880 microscope (Zeiss, Oberkochen, Germany), associated with a thermostated chamber at 37 °C (Zeiss). Cells were imaged with a 40X oil objective using 405 and 633 lasers for coumarin and lysosomes, respectively. At least 5 images with the same magnification were acquired for each condition and analyzed with Fiji ImageJ software (ImageJ, Wayne Rasband National Institutes of Health). A JACoP plugin was used for colocalization analysis and Pearson's coefficient.

3. Results and discussion

3.1. Synthesis and characterization of compounds

The stereoselective synthesis of three novels fluorescent glycoconjugates is realized following two different approaches: vinyl epoxides **10α** and **9β** were used as versatile glycosyl donors [45–48] to access D-Manno and D-Gulo configurations of the glycoconjugated coumarins **17b** and **18a** respectively(Scheme 3), while 2,3,4,6-tetra-*O*-acetyl-α-D-glucopyranosyl bromide was chosen, for a more traditional process, to achieve the D-*Gluco* conjugate **8** (Scheme 2). The fluorescent scaffold consisted of the glycoconjugable coumarin-based fluorophore **4,** bearing a hydroxyl group in C7 position of the coumarin core. This kind of structure determines a push–pull system, thanks to an appropriate functionalization of the coumarin core, realized by the insertion of an electron donor group ("push" portion) in C7 position and an electron attractor group ("pull" portion) in C3 position: this results in an increase of the excitation and emission wavelengths as reported in literature. [49].

The coumarin scaffold **4** was obtained from commercially available cyanuric chloride via a first monosubstitution reaction with ketene dimethyl acetal. The mono-substituted compound **1**, treated with diethyl iminodiacetate in the presence of DIPEA, proceeded to the aromatic nucleophilic substitution of the two remaining chlorine atoms to obtain **2** in almost quantitative yield. Then, the acidic treatment with TFA in aqueous medium converted the ketene functionality into methyl ester **3.** The design of the glyco-conjugable coumarin core was based on the condensation of compound **3** with commercial 2,4-dihydroxybenzaldehyde, through Knoevenagel condensation: the reaction was carried out in anhydrous DMSO and piperidine at 70 °C for 24 h. After acidification of the solution to pH 6–7 and purification by flash chromatography, the desired coumarin derivative **4** was obtained, bearing a glycoconjugable hydroxyl group on carbon C7. The ester functionalities in compound **4** were finally hydrolysed, to obtain the tetracarboxyl-derivative **5**, which represents both the fluorescent coumarin scaffold and the hydrolysis product resulting from the glycolytic enzymes action (Scheme 1).

The D-*Gluco* derivative was prepared using a classic glycoconjugation protocol: 2,4-dihydroxybenzaldehyde acts as the glycosyl acceptor, while 2,3,4,6-tetra-*O*-acetyl-alpha-D-glycopyranosyl bromide is the glycosyl donor, under classic conditions according to literature.[19] Thus, as reported in Scheme 1, α-D-glycopyranosyl bromide and 2,4-dihydroxybenzaldehyde reacted in a suspension of K_2CO_3 and acetone for 3 h at 45 °C to afford regio- and stereoselectively β-glycoside **6.** The expected complete regioselectivity of the glycosylation uniquely on the hydroxyl group in position C4 of the glycosyl acceptor, which is not involved in hydrogen bond with the *ortho* aldeydic group in C1, was confirmed by ROESY map (see ESI). This compound was used for the subsequent addition of triazine derivative **3** in anhydrous DMSO and piperidine at 65 °C for 24 h to give the corresponding 2,3,4,6-tetra-*O*-acetyl-β-D-glucopyranoside coumarin **7**. The final step involved the simultaneous cleavage of the ethyl esters and the fully deacetylation of the hydroxyl groups present in the glucose moiety of compound **7**, to afford final compound **8**, by treatment with a freshly prepared solution of MeONa in MeOH followed by acidic controlled quenching at pH 5.0 with amberlite resin IR120.

The complete conversion was confirmed by ESI-MS and ^1H NMR spectra (see ESI). However, while the increased hydrophilicity due to the conjugation with a fully deprotected monosaccharide helped the water solubility and facilitated the administration in cells experiments, it could affect its ability to interact with lipids in cell membranes and potentially limits its penetration and distribution in cells or tissues. In addition, the chance to investigate the effect of different configurations other than D-Glucose and the presence of a more lipophilic group on the carbohydrate moiety was rather appealing to us in order to evaluate the specificity of action of differently conjugated probes.

In order to control the lipophilicity and assess different absolute configurations, we decided to use the vinyl epoxides **10α** and **9β**, as glycosyl donors (Scheme 2) for the synthesis of glycoconjugates **17β** e **18α.** The glycal building blocks, were extensively investigated by us in the last decades as efficient glycosyl donors.[50–54] In particular, the glycal derived glycosyl donor systems **10α** and **9β** are characterized by a unique reactivity: in the presence of nucleophiles such as alcohols, they are able to undergo a completely 1,4-regio- and stereoselective conjugate addition process, yielding 2,3-unsaturated glycosides with the same configuration as the starting epoxide (i.e. from epoxide **10α** are obtained only 2,3-unsaturated α-glycosides).[14-17] Then, 2,4-dihydroxybenzaldehyde was added to a solution of vinyl epoxide **10α** or **9β**, prepared *in*

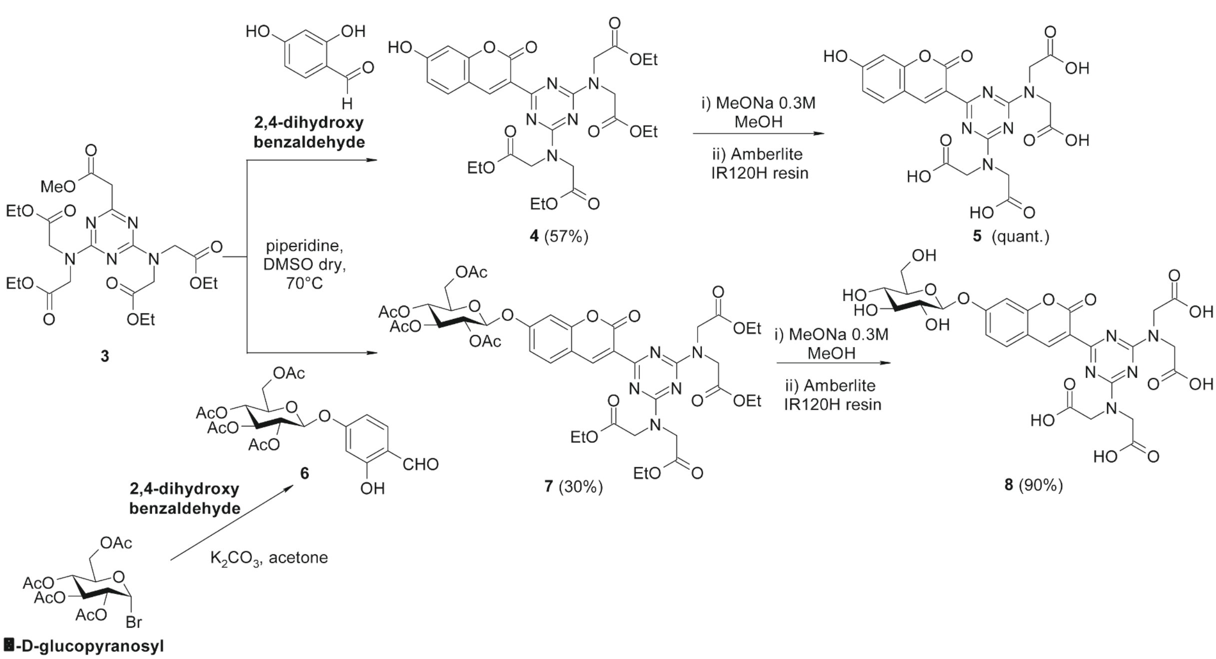

Scheme 1. Synthetic pathway for compounds **5** and **8**.

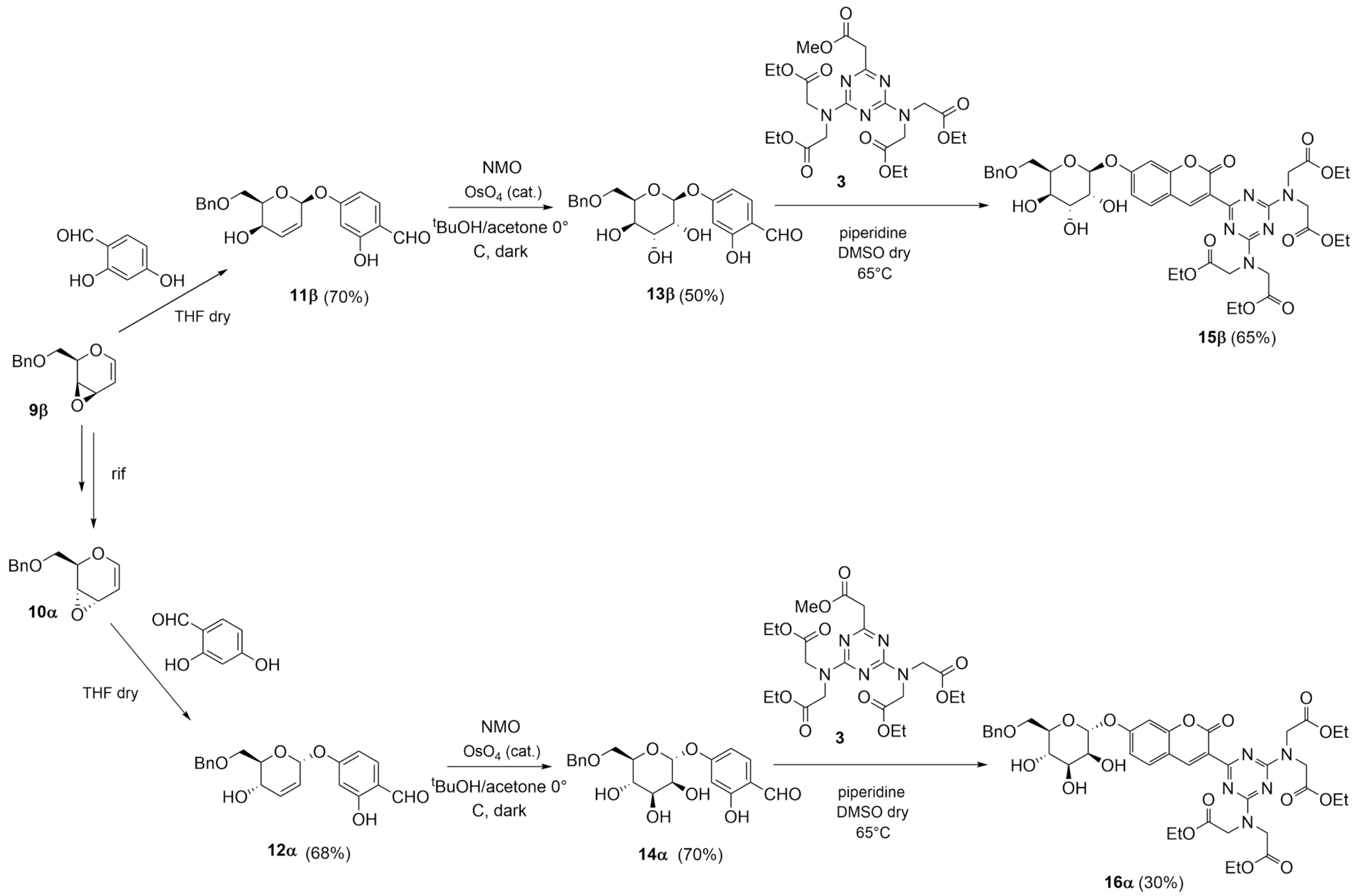

Scheme 2. Synthetic pathway for compounds **15β** and **16α**.

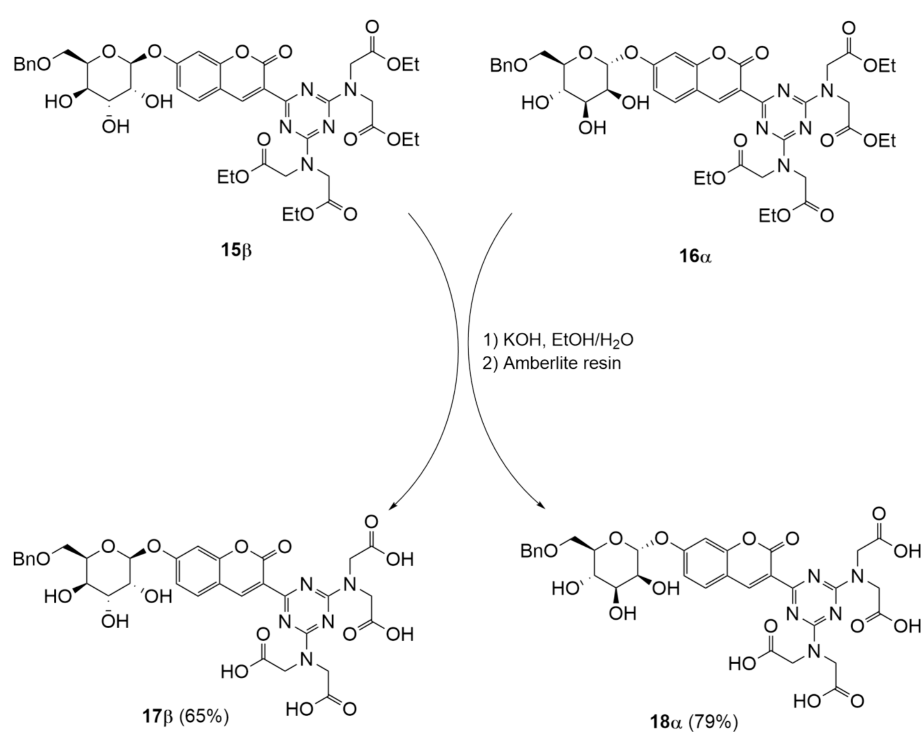

Scheme 3. .Synthetic pathway for compounds **17β** and **18α**.

situ by cyclization with *t*-BuOK of the corresponding *trans*-hydroxy mesylate,[14] obtaining the glycoconjugated derivatives **11β** and **12α**, in excellent yields (also in this case, the expected complete regioselectivity of the glycosylation uniquely on the hydroxyl group in position C4 of the glycosyl acceptor was assessed by NMR, see ESI). Subsequently, the double bond present in **11β** and **12α** was dihydroxylated using OsO_4/*N*-methylmorpholine *N*-oxide (NMMO) according to a previously optimised protocol[16] to give derivatives **13β** and **14α**. The final coumarin core (**15β** and **16α**) was, then, obtained by Knoevenagel condensation with the triazine scaffold **3**. The final step involved the cleavage of the ethyl esters on the triazine moiety to afford glycoconjugates **17β** (β-D-Gulo configuration) and **18α** (α-D-Manno configuration) (Scheme 3), the identity and purity of these final compounds were confirmed by ESI-MS and by ^{1}H NMR spectra (see ESI). While the *gluco*-derivative **8** had been obtained without protecting groups, we decided to avoid the final hydrogen-catalyzed deprotection step due to the sensitivity of these intermediates (especially of the coumarin unit) to hydrogenation conditions. Moreover, recent findings demonstrate that the energetic contribution of the hydroxyl group in position 6 to the stabilization of enzyme-substrate complex is only marginal.[55] Finally, we reasoned that the quite lipophilic benzyl group might enhance cell permeability contributing to overcome one potentially relevant hurdle to overall sensing efficiency. This increase in cell penetration capability has already demonstrated, for benzyl protected compounds, by some of us.[48].

3.2. Fluorescence studies

Fluorescence emission properties of the synthesized substrates were tested to assess their suitability as substrates for enzyme assays. We focused our attention on the spectral properties of **5**, which represents the product deriving from enzymatic cleavage of all the synthesized glycocoumarins (Fig. 1), and the reporter of glycosidase activity. We found that **5** presents a complex response to pH. As shown in Fig. 1, absorption profile changes from acidic to basic pH with a nonlinear trend, giving rise to two different peaks centred around 400 and 450 nm. This is foreseeable in view of the multiple acid-base equilibrium present on triazine ring and that involve the hydroxyl group in position 7 on coumarin ring. Conversely, fluorescence emission upon excitation at 400 nm is more conventional, with two emission peaks centered at 450 and 475 nm. Intriguingly, there is a huge change in fluorescence emission at physiologic pH range (4.5–7.5), an attractive feature in view of the desired role as intracellular pH sensor with low spontaneous background emission. Appropriate choice of two channels (410–450 nm and 460–600 nm) provides a ratiometric response to pH, a feature which is particularly interesting in view of its potential use in cells. Fluorescence quantum yield of compound 5, measured using quinine sulphate as a reference, is strongly pH-dependent. In physiologic range (4.5–8.5) it increases steadily with a sigmoidal curve (see supporting information) raising from 0.04 (pH 4) to 0.35 (pH 8.5), in line with the protonation equilibrium of compound **5**.

The interesting spectroscopic features of **5** are not matched by its glycoconjugate derivatives, likely due to the lack of a mobile proton in position 7 on coumarin ring. This translates in negligible sensitivity to environmental pH. In all cases, glycoside derivatives were characterized by a 1–5 nm shift in absorption and emission (centred at 380 and 460 nm, respectively). Thus, spectroscopic features of glycoside precursors were not further investigated.

Next, we tested the suitability of glyco-conjugated **8**, **18α** and **17β** derivative towards different glycosidases (Fig. 2). Each substrate was tested with the enzyme which is known to be active on the sugar moiety. Additionally, degradation by **α**-glucosidase, which is assumed not to be active on these substrates, was evaluated as negative control. Progress of the cleavage reaction can be easily monitored by the fluorescence increase occurring at 460 nm when the glycosidic portion is cleaved. Interestingly, both **8** and **18α** are sensitive to enzymatic degradation with minimal or no trace of nonspecific cleavage. As expected on the basis of literature findings, the benzyl protecting groups does not inhibit cleavage of the substrate by −glucosidase. D-Gulo derivative showed no increase in fluorescence emission and was no further considered.

3.3. In vitro uptake assessment

Overall, spectrofluorimetric analysis of **8** and **18α** clearly indicates that they can be considered convenient probes for *in vitro* sensing of enzymatic activity. It is widely reported that cancer cells show severely altered enzymatic activities, due to their hampered metabolism. In particular, for our experiments we used two cell lines: mouse embryonic fibroblasts (MEF) are normal cells widely used to make comparisons with other lines that are instead tumoral,[56,57] and GL261 a glioblastoma murine cell lines which is reported to overexpress glucose and mannose receptors.[58] In particular, we chose to test our probes on glioblastoma because in the future they could also be used for the diagnosis of brain cancers, which are notoriously difficult to reach due to the presence of the blood–brain barrier (BBB). This prompted us to further evaluate the suitability of these probes as real time intracellular sensors of cancer metabolism. Notably, use of glycosylated probes could enhance our capability to discriminate between tumor and control cells by synergistically acting at two levels. First, the reported greater avidity of cancer cells for glycosylated products would improve uptake of the probe, and second, increased glycosylase activity would further enhance conversion of the substrate in a fluorescent reporter. The two combined effects are expected to provide a significant selectivity towards tumor cells.

To validate this hypothesis, we set up two different assays. First, we determined subcellular localization of the administered probes by means of confocal fluorescence microscopy (Fig. 3). We observed that the probes accumulate in cells leading to a peculiar pattern that stains several cell organelles, in agreement with the reported intracellular distribution of analogous derivatives.[42] Interestingly, the pH sensing capability of the probes allowed selective staining of cell cytoplasm and intracellular organelles, in keeping with the pH-dependent brightness of the probe. When examining the pH at whole-cell level, no significant variations were observed between tumor and control cells, with a sensed pH centred around 6.5.[42] Co-localization of the signal from the probes with lysosome markers (Lysotracker) confirmed that lysosomes are stained by the probes, along with several other organelles of similar size that, based on the reported pH, could be tentatively ascribed to late endosomes. This observation was confirmed by high values of Person's coefficient of 0.80 ± 0.06 and 0.65 ± 0.1 for cancer and control cells, respectively.

Similarity in the sensed pH at these organelles in cancer and control cells is reasonable in view of the reported literature on tumor metabolism (Fig. 4). Interestingly, fluorescence increases due to the low, yet measurable, shift in pH between intracellular and external compartments lead to an important signal ratio of 5:1 between cells and background even in unwashed media (i.e. in culture media that contain up to 100 μM of the probe).

This measurement of intracellular pH proves also that the probe is effectively cleaved upon internalization in the cells. In fact, glycoside-derivatized precursors are pH insensitive and would not be able to provide a readout in terms of fluorescence change within the cells.

A quantitative evaluation of probe uptake was then performed in a plate-based assay. Derivatives **8** and **18α** were incubated in the presence of tumor and control cells, both in high glucose and low glucose conditions. Fluorescence increase was monitored quantitatively with a plate-reader, and results were normalized to the control cells (Fig. 5). Results clearly indicate a considerable fluorescence increase in tumor vs. control cells (fold change: 2.25 and 2.94 for **8** and **18α**, respectively) in the case of low glucose incubation. Furthermore, all treatments in low glucose condition lead to statistically significant fold changes relative to 1, indicating that the probes are preferentially internalized in tumor

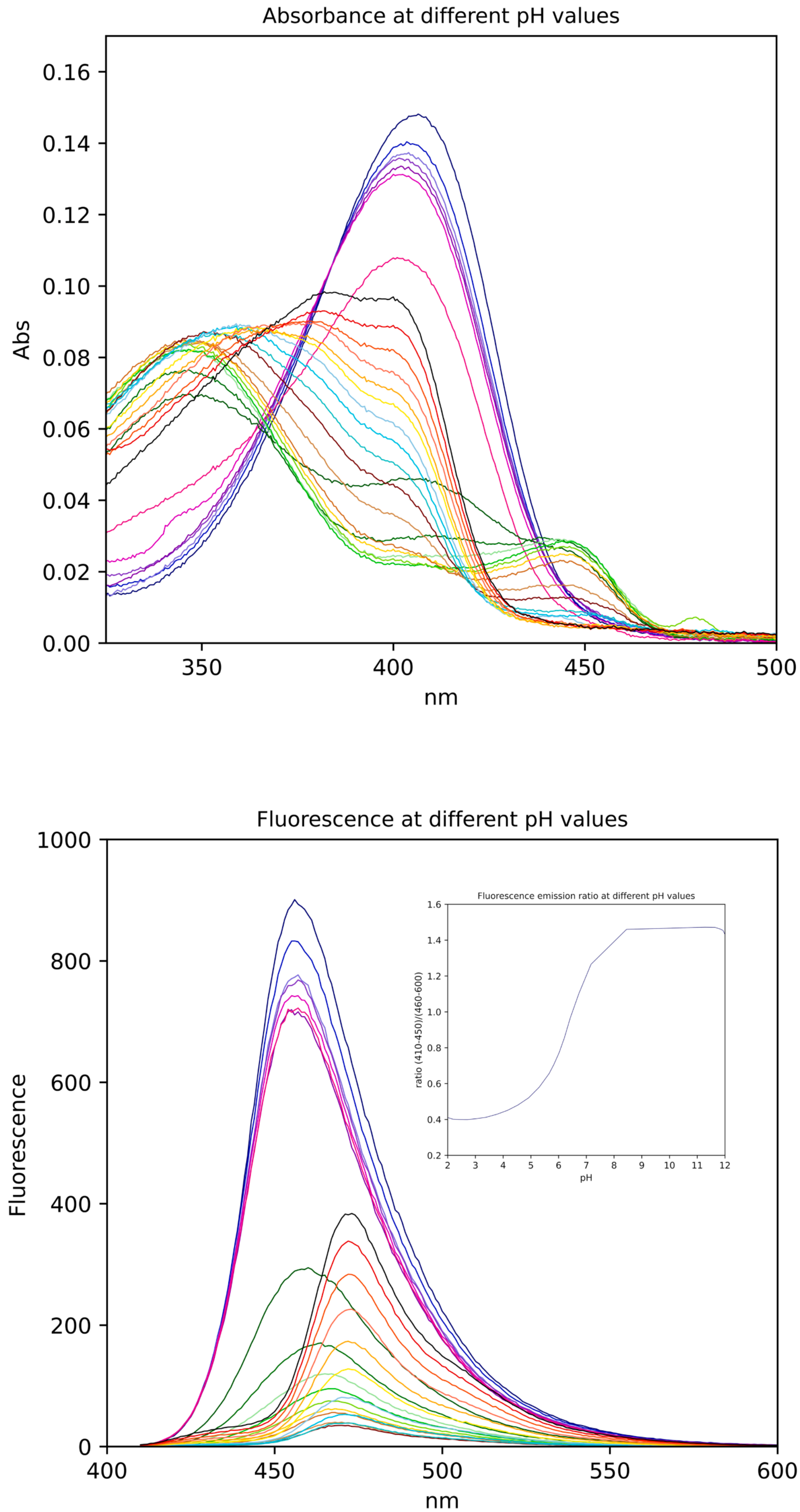

Fig. 1. Fluorescence emission properties of all the synthesized substrates. A) Absorbance spectra of compound **5** at different pH. B) Fluorescent emission spectra of compound **5** at different pH. C) Inset of ratio at different pH of fluorescent spectra emission of **5** between 410–450 nm and 460–600 nm range.

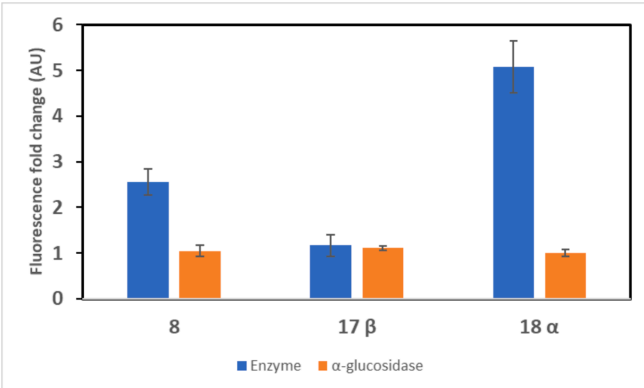

Fig. 2. Fold change in fluorescence emission upon incubation of substrates with the corresponding enzymes. **β**-glucosidase was used for **8** and **17β**, mannosidase for **18α**. In all cases, **α**–glucosidase was considered as negative control (n = 3 for all measurements). The fluorescence was measured at 37 °C for 1 h and the fold change was measured respect to the initial fluorescence measured at time 0 h before adding the substrate to the reaction mixture.

cells compared with control. This significance is maintained, in high glucose condition, only by *manno*-derivative, suggesting the presence of an internalization pathway different from glucose transporters. Fold change between tumor and control cell is markedly lowered when incubation is performed in high glucose condition, in keeping with the competitive uptake of glucose from the medium (statistical significance at $p < 0.01$ between high glucose and low glucose conditions). It is in fact known that GLUT1 transporters are also effective on mannose derivatives.[14] This proves that probe uptake is controlled by cell uptake mechanisms, and it is not a nonspecific process. For the same reason, administration of high concentration of probe (100 μM) lowers the difference between probe uptake in tumor and control cells, in line with the possibility that cell transport mechanisms are saturated. Note that, in these conditions, the effect of glucose concentration in the medium is negligible, as testified by the loss of significance between experiments conducted in high glucose and low glucose conditions (Fig. 5).

A comparison of our results with those already described in the literature highlights that uses fluorescent or fluorogenic probes to discriminate between physiologic and tumor cells. Carbohydrate-functionalized coumarins have been used to distinguish between physiologic, pre-tumoral, and tumoral cells. The proposed mechanism exploits the reported overexpression of GLUT5 transporters, specific for fructose, in tumor cells compared with physiologic ones. This translates in a huge increase in fluorescence emission of more than 20 folds between control and tumor cells.[38] The same strategy was later applied to mannitol-functionalized activatable rhodamine B derivatives.[39] Our strategy does not reach the response factor of these fructose-functionalized probes; however, we our approach opens the way to exploiting different transporters to further increase the number of deliverable probes. The effect of glycoside identity in steering probe internalization selectivity has in fact received considerably less attention compared to that devoted to the engineering of novel fluorophores.

4. Conclusion

In conclusion, we designed a new family of glycoconjugates which have the double feature of allowing preferential uptake in tumor cells compared with control fibroblasts, joined with pH sensitive fluorescence emission and strong solvatochromism. These features act synergistically in improving signal to contrast ratio when the probe is administered to living cells, making possible to distinguish tumor cells without time-

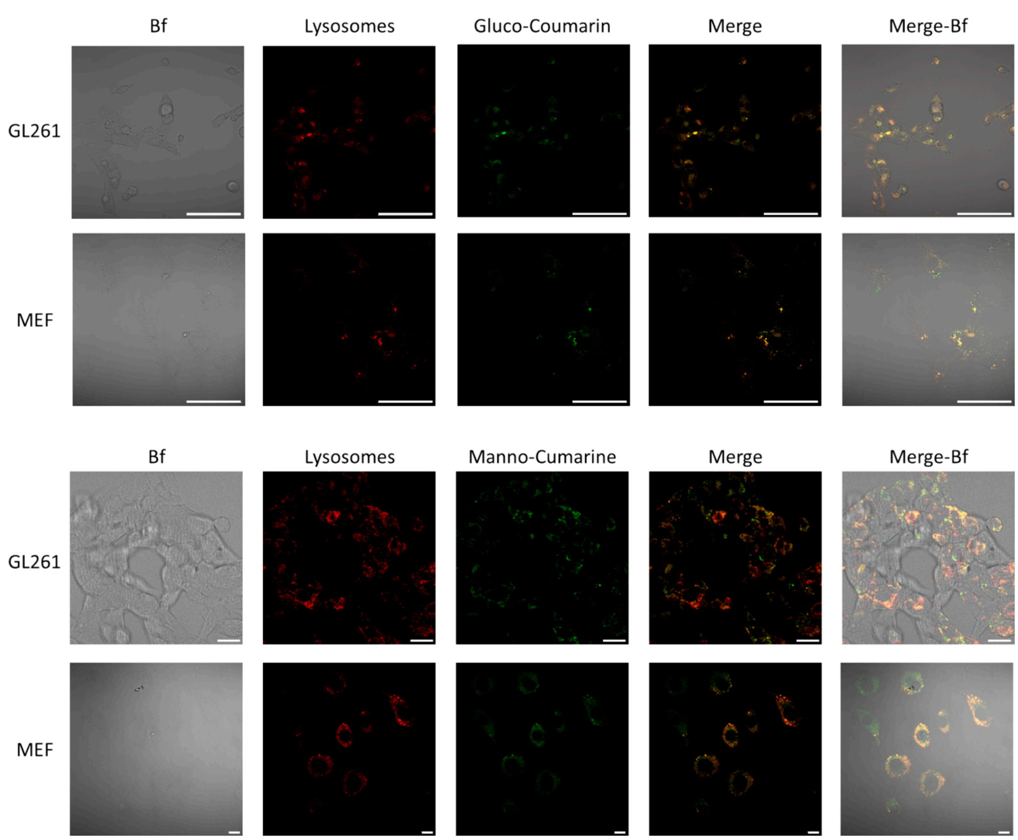

Fig. 3. Cellular localization of **8** (top) and **18α** (bottom) in tumoral (GL261) and control (MEF) cell lines. Cells were seeded and treated with fluorogenic derivatives at a final concentration of 10 μM and lysotracker for 1 h at 37 °C. Cells were then washed with PBS and imaged. At least 10 images were acquired for each sample. Scale bar: 50 μm.

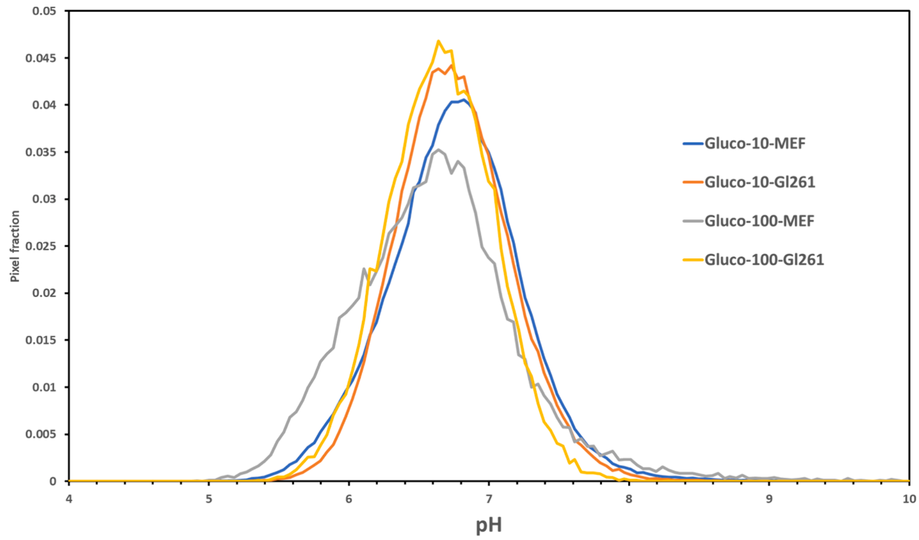

Fig. 4. Intracellular pH signalled by probe **8**.

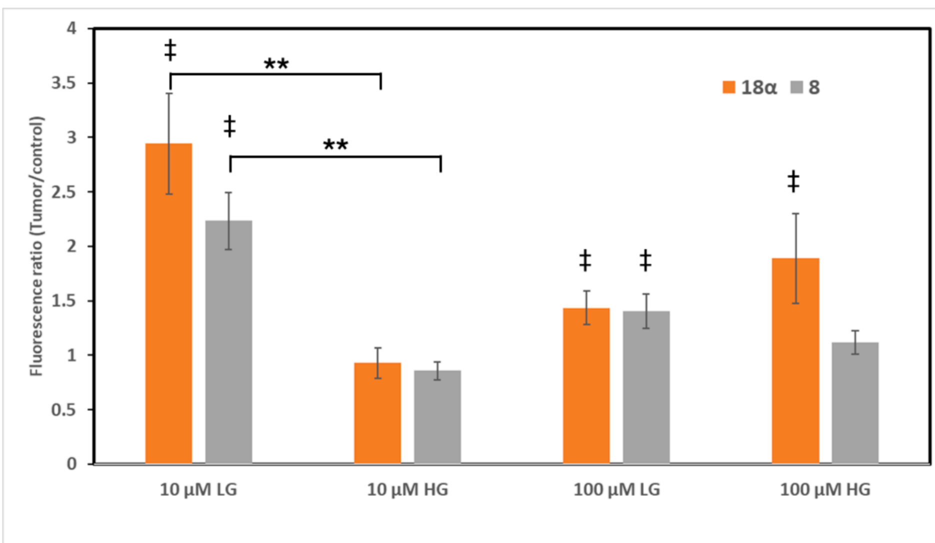

Fig. 5. Fold change in fluorescence intensity for both probes in tumor vs. control cells. Cells were treated with 10 or 100 μM of the probes in medium containing low (1gr/L) or high (4,5gr/L) concentration of glucose. Fluorescence changes were measure in a plate reader and the ratio between tumor and control cells was measured after 2 h at 37 °C. Cells with LG or HG medium and without the probes were used as negative control. **: $p < 0.01$; ‡: $p < 0.05$ relative to 1 (that indicates equal uptake between tumor and control cells).

consuming washing procedures. Compared with other conceptually similar probes, our structures are distinct in that they are based on glucose residue as internalization driver, and to the possibility to report on intracellular physico-chemical proterties (such as pH), potentially providing new insights in tumor cell biochemistry. In perspective, this could be exploited in the engineering of fluorogenic systems for image-guided surgical procedures.

Declaration of competing interest

The authors declare that they have no known competing financial interests or personal relationships that could have appeared to influence the work reported in this paper.

Appendix A. Supplementary data

Supplementary data to this article can be found online at https://doi.org/10.1016/j.bioorg.2024.107836.

References

[1] S.P. Mathupala, A. Rempel, P.L. Pedersen, Aberrant Glycolytic Metabolism of Cancer Cells: A Remarkable Coordination of Genetic, Transcriptional, Post-translational, and Mutational Events That Lead to a Critical Role for Type II Hexokinase, J. Bioenerg. Biomembr. 29 (1997) 339–343, https://doi.org/10.1023/A:1022494613613.
[2] G. Bononi, S. Masoni, V. Di Bussolo, T. Tuccinardi, C. Granchi, F. Minutolo, Historical perspective of tumor glycolysis: A century with Otto Warburg, Semin. Cancer Biol. 86 (2022) 325–333, https://doi.org/10.1016/j.semcancer.2022.07.003.
[3] P. Vaupel, H. Schmidberger, A. Mayer, The Warburg effect: essential part of metabolic reprogramming and central contributor to cancer progression, Int. J. Radiat Biol. 95 (2019) 912–919, https://doi.org/10.1080/09553002.2019.1589653.
[4] J. Zheng, Energy metabolism of cancer: Glycolysis versus oxidative phosphorylation (Review), Oncol. Lett. 4 (2012) 1151–1157, https://doi.org/10.3892/ol.2012.928.

[5] M. Pliszka, L. Szablewski, Glucose Transporters as a Target for Anticancer Therapy, Cancers 13 (2021) 4184, https://doi.org/10.3390/cancers13164184.

[6] O.E. Nieweg, E.E. Kim, W.-H. Wong, W.F. Broussard, S.E. Singletary, G. N. Hortobagyi, R.S. Tilbury, Positron emission tomography with fluorine-18-deoxyglucose in the detection and staging of breast cancer, Cancer 71 (1993) 3920–3925, https://doi.org/10.1002/1097-0142(19930615)71:12<3920::AID-CNCR2820711220>3.0.CO;2-N.

[7] T. Bury, A. Barreto, F. Daenen, N. Barthelemy, B. Ghaye, P. Rigo, Fluorine-18 deoxyglucose positron emission tomography for the detection of bone metastases in patients with non-small cell lung cancer, Eur. J. Nucl. Med. Mol. Imaging 25 (1998) 1244–1247, https://doi.org/10.1007/s002590050291.

[8] F.G. Duhaylongsod, V.J. Lowe, E.F. Patz, A.L. Vaughn, R.E. Coleman, W.G. Wolfe, Lung tumor growth correlates with glucose metabolism measured by fluoride-18 fluorodeoxyglucose positron emission tomography, Ann. Thorac. Surg. 60 (1995) 1348–1352, https://doi.org/10.1016/0003-4975(95)00754-9.

[9] P. Swietach, What is pH regulation, and why do cancer cells need it? Cancer Metastasis Rev 38 (2019) 5–15, https://doi.org/10.1007/s10555-018-09778-x.

[10] P.A. Schornack, R.J. Gillies, Contributions of Cell Metabolism and H+ Diffusion to the Acidic pH of Tumors, Neoplasia 5 (2003) 135–145, https://doi.org/10.1016/S1476-5586(03)80005-2.

[11] M.L. Goodwin, L.B. Gladden, M.W.N. Nijsten, K.B. Jones, Lactate and Cancer: Revisiting the Warburg Effect in an Era of Lactate Shuttling, Front. Nutr. 1 (2015), https://doi.org/10.3389/fnut.2014.00027.

[12] S. Pavlides, D. Whitaker-Menezes, R. Castello-Cros, N. Flomenberg, A. K. Witkiewicz, P.G. Frank, M.C. Casimiro, C. Wang, P. Fortina, S. Addya, R. G. Pestell, U.E. Martinez-Outschoorn, F. Sotgia, M.P. Lisanti, The reverse Warburg effect: Aerobic glycolysis in cancer associated fibroblasts and the tumor stroma, Cell Cycle 8 (2009) 3984–4001, https://doi.org/10.4161/cc.8.23.10238.

[13] T.L. Dayton, T. Jacks, M.G. Vander Heiden, PKM 2, cancer metabolism, and the road ahead, EMBO Rep. 17 (2016) 1721–1730, https://doi.org/10.15252/embr.201643300.

[14] M. Alquraishi, D.L. Puckett, D.S. Alani, A.S. Humidat, V.D. Frankel, D.R. Donohoe, J. Whelan, A. Bettaieb, Pyruvate kinase M2: A simple molecule with complex functions, Free Radic. Biol. Med. 143 (2019) 176–192, https://doi.org/10.1016/j.freeradbiomed.2019.08.007.

[15] A.R. Mitchell, M. Yuan, H.P. Morgan, I.W. McNae, E.A. Blackburn, T. Le Bihan, R. A. Homem, M. Yu, G.J. Loake, P.A. Michels, M.A. Wear, M.D. Walkinshaw, Redox regulation of pyruvate kinase M2 by cysteine oxidation and S-nitrosation, Biochem. J 475 (2018) 3275–3291, https://doi.org/10.1042/BCJ20180556.

[16] X. Zhang, Y. Lin, R.J. Gillies, Tumor pH and Its Measurement, J Nucl Med 51 (2010) 1167–1170, https://doi.org/10.2967/jnumed.109.068981.

[17] Y. Urano, D. Asanuma, Y. Hama, Y. Koyama, T. Barrett, M. Kamiya, T. Nagano, T. Watanabe, A. Hasegawa, P.L. Choyke, H. Kobayashi, Selective molecular imaging of viable cancer cells with pH-activatable fluorescence probes, Nat Med 15 (2009) 104–109, https://doi.org/10.1038/nm.1854.

[18] L.E. Gerweck, K. Seetharaman, Cellular pH Gradient in Tumor versus Normal Tissue: Potential Exploitation for the Treatment of Cancer, (1996) 6.

[19] S. Keereweer, J.D.F. Kerrebijn, P.B.A.A. van Driel, B. Xie, E.L. Kaijzel, T.J. A. Snoeks, I. Que, M. Hutteman, J.R. van der Vorst, J.S.D. Mieog, A.L. Vahrmeijer, C.J.H. van de Velde, R.J. Baatenburg de Jong, C.W.G.M. Löwik, Optical Image-guided Surgery—Where Do We Stand? Mol Imaging Biol 13 (2011) 199–207, https://doi.org/10.1007/s11307-010-0373-2.

[20] X. Li, C. Schumann, H.A. Albarqi, C.J. Lee, A.W.G. Alani, S. Bracha, M. Milovancev, O. Taratula, O. Taratula, A Tumor-Activatable Theranostic Nanomedicine Platform for NIR Fluorescence-Guided Surgery and Combinatorial Phototherapy, Theranostics 8 (2018) 767–784, https://doi.org/10.7150/thno.21209.

[21] R. Blau, Y. Epshtein, E. Pisarevsky, G. Tiram, S.I. Dangoor, E. Yeini, A. Krivitsky, A. Eldar-Boock, D. Ben-Shushan, H. Gibori, A. Scomparin, O. Green, Y. Ben-Nun, E. Merquiol, H. Doron, G. Blum, N. Erez, R. Grossman, Z. Ram, D. Shabat, R. Satchi-Fainaro, Image-guided surgery using near-infrared Turn-ON fluorescent nanoprobes for precise detection of tumor margins, Theranostics 8 (2018) 3437–3460, https://doi.org/10.7150/thno.23853.

[22] A. Nabavi, H. Thurm, B. Zountsas, T. Pietsch, H. Lanfermann, U. Pichlmeier, M. Mehdorn, Five-aminolevulinic acid for fluorescence-guided resectionof recurrent malignant gliomas: a phase II study, Neurosurgery 65 (2009) 1070–1077, https://doi.org/10.1227/01.NEU.0000360128.03597.C7.

[23] W. Stummer, U. Pichlmeier, T. Meinel, O.D. Wiestler, F. Zanella, H.-J. Reulen, Fluorescence-guided surgery with 5-aminolevulinic acid for resection of malignant glioma: a randomised controlled multicentre phase III trial, Lancet Oncol. 7 (2006) 392–401, https://doi.org/10.1016/S1470-2045(06)70665-9.

[24] S. Zhao, J. Wu, C. Wang, H. Liu, X. Dong, C. Shi, C. Shi, Y. Liu, L. Teng, D. Han, X. Chen, G. Yang, L. Wang, C. Shen, H. Li, Intraoperative Fluorescence-Guided Resection of High-Grade Malignant Gliomas Using 5-Aminolevulinic Acid-Induced Porphyrins: A Systematic Review and Meta-Analysis of Prospective Studies, PLoS One 8 (2013) e63682.

[25] Q.-J. Duan, Z.-Y. Zhao, Y.-J. Zhang, L. Fu, Y.-Y. Yuan, J.-Z. Du, J. Wang, Activatable fluorescent probes for real-time imaging-guided tumor therapy, Adv. Drug Deliv. Rev. 196 (2023) 114793, https://doi.org/10.1016/j.addr.2023.114793.

[26] K.A. White, K. Kisor, D.L. Barber, Intracellular pH dynamics and charge-changing somatic mutations in cancer, Cancer Metastasis Rev 38 (2019) 17–24, https://doi.org/10.1007/s10555-019-09791-8.

[27] B. Kotoński, J. Wilczek, J. Madej, A. Zarzycki, J. Hutny, Activity of glycogen depolymerizing enzymes in extracts from brain tumor tissue (anaplastic astrocytoma and glioblastoma multiforme), Acta Biochim Pol 48 (2001) 1085–1090, https://doi.org/10.18388/abp.2001_3869.

[28] D. Wei, D.M. Engelman, Y.K. Reshetnyak, O.A. Andreev, Mapping pH at Cancer Cell Surfaces, Mol Imaging Biol 21 (2019) 1020–1025, https://doi.org/10.1007/s11307-019-01335-4.

[29] T. Zhang, F. Huo, W. Zhang, J. Chao, C. Yin, Ultra-pH-sensitive sensor for visualization of lysosomal autophagy, drug-induced pH alteration and malignant tumors microenvironment, Sensors and Actuators b: Chemical 345 (2021) 130393, https://doi.org/10.1016/j.snb.2021.130393.

[30] L. Wang, C. Li, pH responsive fluorescence nanoprobe imaging of tumors by sensing the acidic microenvironment, J. Mater. Chem. 21 (2011) 15862, https://doi.org/10.1039/c1jm12072g.

[31] L. Dong, M.-Y. Zhang, H.-H. Han, Y. Zang, G.-R. Chen, J. Li, X.-P. He, S. Vidal, A general strategy to the intracellular sensing of glycosidases using AIE-based glycoclusters, Chem. Sci. 13 (2022) 247–256, https://doi.org/10.1039/D1SC05057E.

[32] K. Fujita, M. Kamiya, T. Yoshioka, A. Ogasawara, R. Hino, R. Kojima, H. Ueo, Y. Urano, Rapid and Accurate Visualization of Breast Tumors with a Fluorescent Probe Targeting α-Mannosidase 2C1, ACS Cent. Sci. 6 (2020) 2217–2227, https://doi.org/10.1021/acscentsci.0c01189.

[33] K. Fujita, M. Kamiya, Y. Urano, Rapid and Sensitive Detection of Cancer Cells with Activatable Fluorescent Probes for Enzyme Activity, in: S.-B. Kim (Ed.), Live Cell Imaging, Springer US, New York, NY, 2021: pp. 193–206. https://doi.org/10.1007/978-1-0716-1258-3_17.

[34] X. Chai, H.-H. Han, A.C. Sedgwick, N. Li, Y. Zang, T.D. James, J. Zhang, X.-L. Hu, Y. Yu, Y. Li, Y. Wang, J. Li, X.-P. He, H. Tian, Photochromic Fluorescent Probe Strategy for the Super-resolution Imaging of Biologically Important Biomarkers, J. Am. Chem. Soc. 142 (2020) 18005–18013, https://doi.org/10.1021/jacs.0c05379.

[35] J. Zhang, Y. Fu, H.-H. Han, Y. Zang, J. Li, X.-P. He, B.L. Feringa, H. Tian, Remote light-controlled intracellular target recognition by photochromic fluorescent glycoprobes, Nat Commun 8 (2017) 987, https://doi.org/10.1038/s41467-017-01137-8.

[36] M. Wu, D. Gong, Y. Zhou, Z. Zha, X. Xia, Activatable probes with potential for intraoperative tumor-specific fluorescence-imaging guided surgery, J. Mater. Chem. B 11 (2023) 9777–9797, https://doi.org/10.1039/D3TB01590D.

[37] S. Chen, X. Ma, L. Wang, Y. Wu, Y. Wang, W. Fan, S. Hou, Design and application of lysosomal targeting pH-sensitive β-galactosidase fluorescent probe, Sens. Actuators B 379 (2023) 133272, https://doi.org/10.1016/j.snb.2022.133272.

[38] S. Kannan, V. Begoyan, J. Fedie, S. Xia, Ł. Weseliński, M. Tanasova, S. Rao, Metabolism-Driven High-Throughput Cancer Identification with GLUT5-Specific Molecular Probes, Biosensors 8 (2018) 39, https://doi.org/10.3390/bios8020039.

[39] M.M. Soma Nyansa, A. Oronova, N. Gora, M.R. Geborkoff, N.R. Ostlund, D.R. Fritz, T. Werner, M. Tanasova, Turn-on Rhodamine Glycoconjugates Enable Real-Time GLUT Activity Monitoring in Live Cells and In Vivo, Chemical & Biomedical Imaging 1 (2023) 637–647. https://doi.org/10.1021/cbmi.3c00063.

[40] G. Signore, R. Nifosì, L. Albertazzi, B. Storti, R. Bizzarri, Polarity-Sensitive Coumarins Tailored to Live Cell Imaging, J. Am. Chem. Soc. 132 (2010) 1276–1288, https://doi.org/10.1021/ja9050444.

[41] S. Di Pietro, D. Iacopini, A. Moscardini, R. Bizzarri, M. Pineschi, V. Di Bussolo, G. Signore, New Coumarin Dipicolinate Europium Complexes with a Rich Chemical Speciation and Tunable Luminescence, Molecules 26 (2021) 1265, https://doi.org/10.3390/molecules26051265.

[42] D. Iacopini, A. Moscardini, F. Lessi, V. Di Bussolo, S. Di Pietro, G. Signore, Coumarin-based fluorescent biosensor with large linear range for ratiometric measurement of intracellular pH, Bioorg. Chem. 105 (2020) 104372, https://doi.org/10.1016/j.bioorg.2020.104372.

[43] M. Macchia, F. Salvetti, S. Bertini, V. Di Bussolo, L. Gattuso, M. Gesi, M. Hamdan, K.-N. Klotz, T. Laragione, A. Lucacchini, F. Minutolo, S. Nencetti, C. Papi, D. Tuscano, C. Martini, 7-Nitrobenzofurazan (NBD) derivatives of 5′-N-ethylcarboxamidoadenosine (NECA) as new fluorescent probes for human A3 adenosine receptors, Bioorg. Med. Chem. Lett. 11 (2001) 3023–3026, https://doi.org/10.1016/S0960-894X(01)00610-2.

[44] S. Fortunato, C. Lenzi, C. Granchi, V. Citi, A. Martelli, V. Calderone, S. Di Pietro, G. Signore, V. Di Bussolo, F. Minutolo, First Examples of H_2 S-Releasing Glycoconjugates: Stereoselective Synthesis and Anticancer Activities, Bioconjugate Chem. 30 (2019) 614–620, https://doi.org/10.1021/acs.bioconjchem.8b00808.

[45] V. Di Bussolo, M. Caselli, M.R. Romano, M. Pineschi, P. Crotti, Regio- and Stereoselectivity of the Addition of O -, S -, N -, and C -Nucleophiles to the β Vinyl Oxirane Derived from d -Glucal, J. Org. Chem. 69 (2004) 8702–8708, https://doi.org/10.1021/jo048981b.

[46] V. Di Bussolo, M. Caselli, M.R. Romano, M. Pineschi, P. Crotti, Stereospecific Uncatalyzed α- O -Glycosylation and α- C -Glycosidation by Means of a New d -Gulal-Derived α Vinyl Oxirane, J. Org. Chem. 69 (2004) 7383–7386, https://doi.org/10.1021/jo0491152.

[47] V. Di Bussolo, E.C. Calvaresi, C. Granchi, L. Del Bino, I. Frau, M.C. Dasso Lang, T. Tuccinardi, M. Macchia, A. Martinelli, P.J. Hergenrother, F. Minutolo, Synthesis and biological evaluation of non-glucose glycoconjugated N-hydroxyindole class LDH inhibitors as anticancer agents, RSC Adv. 5 (2015) 19944–19954. https://doi.org/10.1039/C5RA00946D.

[48] D. Iacopini, J. Vančo, S. Di Pietro, V. Bordoni, S. Zacchini, F. Marchetti, Z. Dvořák, T. Malina, L. Biancalana, Z. Trávníček, V. Di Bussolo, New glycoconjugation strategies for Ruthenium(II) arene complexes via phosphane ligands and assessment of their antiproliferative activity, Bioorg. Chem. 126 (2022) 105901, https://doi.org/10.1016/j.bioorg.2022.105901.

[49] S.K. Lanke, N. Sekar, Coumarin Push-Pull NLOphores with Red Emission: Solvatochromic and Theoretical Approach, J Fluoresc 26 (2016) 949–962, https://doi.org/10.1007/s10895-016-1783-6.

[50] E.C. Calvaresi, C. Granchi, T. Tuccinardi, V. Di Bussolo, R.W. Huigens, H.Y. Lee, R. Palchaudhuri, M. Macchia, A. Martinelli, F. Minutolo, P.J. Hergenrother, Dual Targeting of the Warburg Effect with a Glucose-Conjugated Lactate Dehydrogenase Inhibitor, Chembiochem 14 (2013) 2263–2267, https://doi.org/10.1002/cbic.201300562.

[51] V. Di Bussolo, Y.-J. Kim, D.Y. Gin, Direct Oxidative Glycosylations with Glycal Donors, J. Am. Chem. Soc. 120 (1998) 13515–13516, https://doi.org/10.1021/ja982112k.

[52] V. Di Bussolo, J. Liu, L.G. Huffman, D.Y. Gin, Acetamidoglycosylation with Glycal Donors: A One-Pot Glycosidic Coupling with Direct Installation of the Natural C(2)-N-Acetylamino Functionality, Angew Chem Int Ed Engl 39 (2000) 204–207, https://doi.org/10.1002/(sici)1521-3773(20000103)39:1<204::aid-anie204>3.3.co;2-q.

[53] J.Y. Kim, V. Di Bussolo, D.Y. Gin, Stereoselective synthesis of 2-hydroxy-alpha-mannopyranosides from glucal donors, Org Lett 3 (2001) 303–306, https://doi.org/10.1021/ol006941y.

[54] J. Liu, V. Di Bussolo, D.Y. Gin, C2-Acetamidomannosylation. Synthesis of 2-N-acetylamino-2-deoxy-α-d-mannopyranosides with glucal donors, Tetrahedron Letters 44 (2003) 4015–4018. https://doi.org/10.1016/S0040-4039(03)00871-2.

[55] S. Marana, Molecular basis of substrate specificity in family 1 glycoside hydrolases, IUBMB Life (International Union of Biochemistry and Molecular Biology: Life) 58 (2006) 63–73. https://doi.org/10.1080/15216540600617156.

[56] X. Zha, Z. Hu, S. Ji, F. Jin, K. Jiang, C. Li, P. Zhao, Z. Tu, X. Chen, L. Di, H. Zhou, H. Zhang, NFκB up-regulation of glucose transporter 3 is essential for hyperactive mammalian target of rapamycin-induced aerobic glycolysis and tumor growth, Cancer Lett. 359 (2015) 97–106, https://doi.org/10.1016/j.canlet.2015.01.001.

[57] E.H. Heiss, D. Schachner, K. Zimmermann, V.M. Dirsch, Glucose availability is a decisive factor for Nrf2-mediated gene expression, Redox Biol. 1 (2013) 359–365, https://doi.org/10.1016/j.redox.2013.06.001.

[58] Z. Bao, K. Chen, S. Krepel, P. Tang, W. Gong, M. Zhang, W. Liang, A. Trivett, M. Zhou, J.M. Wang, High Glucose Promotes Human Glioblastoma Cell Growth by Increasing the Expression and Function of Chemoattractant and Growth Factor Receptors, Transl. Oncol. 12 (2019) 1155–1163, https://doi.org/10.1016/j.tranon.2019.04.016.